

DOI: 10.1002/adfm.200500392

# Fabrication of Single-Crystalline Silicon Nanowires by Scratching a Silicon Surface with Catalytic Metal Particles\*\*

By Kuiqing Peng,\* Juejun Hu, Yunjie Yan, Yin Wu, Hui Fang, Ying Xu, Shuitong Lee, and Jing Zhu\*

A novel strategy for preparing large-area, oriented silicon nanowire (SiNW) arrays on silicon substrates at near room temperature by localized chemical etching is presented. The strategy is based on metal-induced (either by Ag or Au) excessive local oxidation and dissolution of a silicon substrate in an aqueous fluoride solution. The density and size of the as-prepared SiNWs depend on the distribution of the patterned metal particles on the silicon surface. High-density metal particles facilitate the formation of silicon nanowires. Well-separated, straight nanoholes are dug along the Si block when metal particles are well dispersed with a large space between them. The etching technique is weakly dependent on the orientation and doping type of the silicon wafer. Therefore, SiNWs with desired axial crystallographic orientations and doping characteristics are readily obtained. Detailed scanning electron microscopy observations reveal the formation process of the silicon nanowires, and a reasonable mechanism is proposed on the basis of the electrochemistry of silicon and the experimental results.

## 1. Introduction

The successful synthesis of carbon nanotubes<sup>[1]</sup> has stimulated much research in nanomaterials, in particular, in semiconducting nanostructures, which are interesting for their novel size- and dimensionality-dependent physical properties, and their potential applications in nanoscale optoelectronics.<sup>[2]</sup> Silicon is the most important semiconducting material, with its contemporary microelectronic technology being one of the greatest successes of the twentieth century. Bulk silicon does not emit visible light, because it is an indirect-bandgap material with a small exciton-binding energy (15 meV). Low-dimensional Si nanostructures, such as quantum dots, nanocrystals, porous silicon, and nanowires can have a direct bandgap, and emit visible light according to the quantum-confinement effect.<sup>[3]</sup> For this reason, a great deal of effort has been invested in preparing these low-dimensional Si nanostructures; their potential applications include the fabrication of Si-based optoelectronic devices. One-dimensional (1D) silicon nanowires

(SiNWs) in particular have been intensely investigated. Much effort has been made to prepare SiNWs by different methods, such as chemical vapor deposition,<sup>[4]</sup> laser ablation,<sup>[5,6]</sup> thermal evaporation decomposition,<sup>[7,8]</sup> supercritical-fluid-liquid-solid (SFLS) synthesis,<sup>[9]</sup> and other methods.<sup>[10]</sup> These methods are quite accessible and well controlled. For example, single-crystalline SiNWs with controlled diameters have been prepared by laser-assisted catalytic growth.<sup>[11]</sup> The axial orientation of SiNWs can be tuned when using the SFLS method.<sup>[9]</sup>

The importance of electrochemistry in Si microelectronic technology has spurred intense research activity.<sup>[12]</sup> In particular, silicon shows novel electrochemical properties in solutions containing hydrofluoric acid: the complex electrochemical etching behavior has raised considerable research interest. Electroless metal deposition (EMD) and electroless etching have been widely investigated, owing to their important applications in the microelectronics industry.<sup>[13]</sup> EMD is often described as a galvanic displacement process that involves the spontaneous oxidation of Si atoms, and the reduction of metal ions to metallic particles and films in the absence of an external source of electric current. The galvanic displacement process can be described using mixed potential theory. Now the EMD technique has been extended to the fabrication of various nanostructures.

Herein, we report the room-temperature fabrication of highly oriented SiNW arrays, and also porous silicon, using simple chemical etching of Si wafers in an aqueous HF solution containing Fe<sup>3+</sup> ions: the process is based on the metal-seed-induced excessive local oxidation and dissolution of Si substrates. This direct approach allows the rapid fabrication of high-quality, well-aligned SiNW arrays with large-area homogeneity and tunable depths. By utilizing this method, single-crystalline SiNWs with desirable crystallographic orientations can be readily and controllably created by the selection of Si wafers with the corresponding crystallographic orientations.<sup>[14]</sup> According to the quantum-confinement effect, accurate axial-ori-

[\*] Dr. K. Q. Peng, Prof. J. Zhu, J. J. Hu, Y. J. Yan, Y. Wu, H. Fang  
Department of Materials Sciences and Engineering  
Tsinghua University  
Beijing 100084 (P.R. China)  
E-mail: kuiqing99@mails.tsinghua.edu.cn;  
jzhu@mail.tsinghua.edu.cn

Dr. K. Q. Peng, Prof. S. T. Lee  
Department of Physics and Materials Science  
Center of Super-Diamond and Advanced Films (COSDAF)  
City University of Hong Kong  
Hong Kong SAR (P.R. China)

Y. Xu  
Institute of Solar Energy Research  
Beijing 100084 (P.R. China)

[\*\*] This work was supported by the Chinese National Natural Science Foundation, the National 973 Project of China, and the National Center for Nanoscience and Technology of China.

entation control of the SiNWs is of importance to materials synthesis and future nanoscale optoelectronic devices that employ silicon. A systematic exploration of the formation mechanism of the as-prepared Si nanostructures was possible, owing to the absence of large quantities of metallic dendrites, which have previously prevented such a study.<sup>[15]</sup> Herein, a mechanism, based on a local microelectrochemical reaction, is proposed according to electrochemical principles and convincing experimental evidence.

## 2. Results and Discussion

### 2.1. Formation of Si Nanowires Using Ag Nanoparticles

Previous studies have shown that luminescent porous silicon can be hydrothermally prepared in an aqueous HF/Fe(NO<sub>3</sub>)<sub>3</sub> solution.<sup>[16]</sup> Generally, the etching of a cleaned Si wafer proceeds very slowly in aqueous HF/Fe(NO<sub>3</sub>)<sub>3</sub> solution at temperatures as low as 50 °C. However, Si etching occurs rapidly when Si substrates covered with Ag-nanoparticle films are immersed in HF/Fe(NO<sub>3</sub>)<sub>3</sub> solution at room temperature. More interestingly, high-quality, oriented SiNW arrays can be produced on Si substrates under optimized etching conditions. Figure 1a

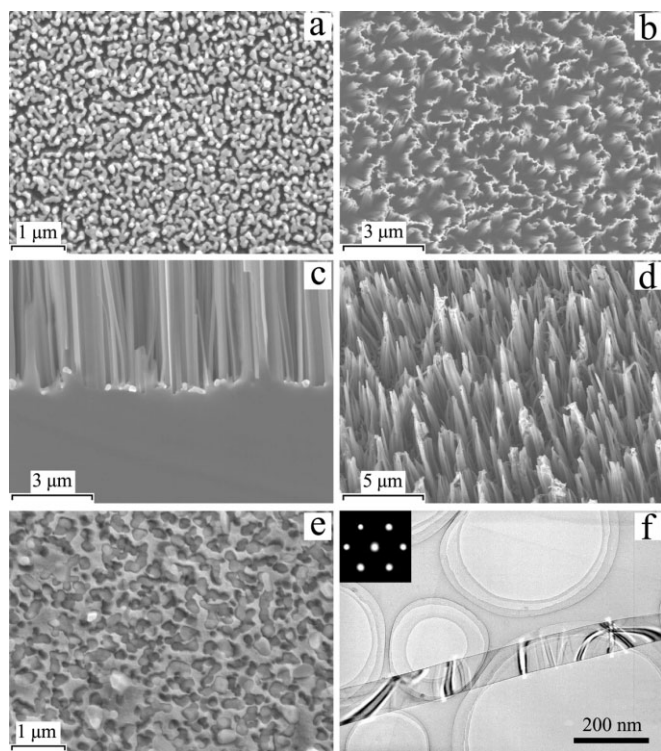


**Figure 1.** a) SEM image of Ag-nanoparticle film deposited onto a p-type Si surface in HF/AgNO<sub>3</sub> for 1 min. b) SEM image of well-aligned nanowire arrays prepared in 5.0 mol L<sup>-1</sup> HF containing 0.02 mol L<sup>-1</sup> Fe(NO<sub>3</sub>)<sub>3</sub>. c) SEM cross-sectional image of the as-synthesized SiNW arrays shown in (b). d) 1D Si microstructure arrays in non-aqueous HF/H<sub>2</sub>O<sub>2</sub> solution. e) The initial stages of a Ag-treated Si substrate synthesized in an ethanol HF/H<sub>2</sub>O<sub>2</sub> solution. f) A single-crystalline Si nanoribbon fabricated from a p-type Si(111) wafer, with the selected-area electron diffraction pattern along the [110] axis shown in the inset.

shows the scanning electron microscopy (SEM) image of a Ag-nanoparticle film deposited onto the surface of a p-type Si(111) wafer by electroless plating in HF/AgNO<sub>3</sub> for 1 min. The deposited nanoparticles tend to form interconnected networks, and there is no major difference in morphology between p- and n-type Si substrates. After the electroless deposition of the Ag-nanoparticle films, the Ag-covered Si substrate was immersed in an aqueous HF/Fe(NO<sub>3</sub>)<sub>3</sub> solution at 50 °C for 30 min. The concentrations of HF and Fe(NO<sub>3</sub>)<sub>3</sub> were 5.0 and 0.02 mol L<sup>-1</sup>, respectively. The as-synthesized sample was black, which implies its possible excellent antireflection ability. SEM observation shows that well-aligned nanowire arrays perpendicular to the surface of the Si substrate were produced (Fig. 1b). Our detailed morphological-evolution investigation has confirmed that Ag nanoparticles gradually sank into the bulk silicon, and that the SiNW arrays gradually emerged with the elapse of treatment time. This sinking behavior of the Ag nanoparticles is clearly shown in a SEM cross-sectional image: many Ag nanoparticles are visible at the interface between the SiNWs and the Si substrate (Fig. 1c). By substituting H<sub>2</sub>O<sub>2</sub> for Fe(NO<sub>3</sub>)<sub>3</sub> in the HF etching solution (using ethanol as the solvent), 1D submicrometer-sized Si structures could also be prepared under appropriate experimental conditions (Fig. 1d). The typical sinking behavior of Ag nanoparticles was observed in the initial stages of exposure to the ethanol HF/H<sub>2</sub>O<sub>2</sub> solution (Fig. 1e). Transmission electron microscopy (TEM) analysis of the as-prepared SiNWs confirmed their single-crystalline Si nature, and revealed that these 1D Si nanostructures have three main shapes: wires, ribbons, and triangles. Most of the 1D Si nanostructures are ribbons, typically 150–250 nm wide. The 1D Si nanostructures with diameters of 10–20 nm are usually round wires. The ends of the 1D Si nanostructures with diameters of 80–150 nm have a triangular cross section. However, it is surprising to see that most of the nanostructures are smooth from top to bottom and that there is almost no diameter modulation along the axis. TEM structural analysis also indicates that the axial orientation of the nanowires is identical to the orientation of the Si wafer used. This means that Si nanowires with a desirable axial orientation can be readily and controllably fabricated by selecting a Si wafer with the corresponding crystallographic orientation.

Our detailed experiments revealed that the electroless Ag deposition in HF/AgNO<sub>3</sub> solution, and the etching behavior of Ag-covered silicon in HF/Fe(NO<sub>3</sub>)<sub>3</sub>, show no significant dependence on the doping type and orientation of the Si wafer used. That is, the etching behavior was nearly identical, regardless of the conduction type and orientation of the Si substrate used. By utilizing this unique etching characteristic, SiNW arrays on different Si substrates were successfully prepared. Figures 2a,b show SEM images of SiNW arrays prepared on an n-type Si(100) substrate and on a p-type Si(100) substrate (Fig. 2b), with resistivities of 3–6 Ω cm. The morphology of the Ag-particle film greatly influenced the etching morphology of the Si wafer. The density and size of the as-prepared SiNWs depended on the distribution pattern of the Ag particles on the Si surface. A high density of Ag particles facilitated the formation of Si nanowires. The size of the SiNWs was closely related to



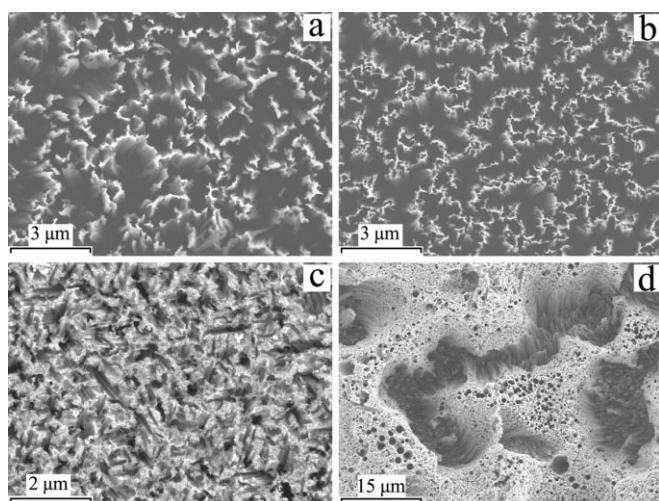


**Figure 2.** SEM observations of as-synthesized samples: a) SEM image of a SiNW array prepared on an n-type Si(100) substrate; b) SiNW array prepared on a p-type Si(100) substrate. c) Si nanostructures prepared with small Ag particles in HF/Fe(NO<sub>3</sub>)<sub>3</sub> solution. d) Disordered porous silicon prepared with high HF concentration.

the space between metal particles, and also the immersion time in the HF solution. For highly dispersed Ag particles separated by a large space, well-separated, straight nanoholes were dug along the Si block. In this case, the porosity and pore size depended on the density and size of the deposited metal particles. In addition, by using a Ag-particle film prepared with a short electroless deposition time (for example, 10 s), which would lead to small particles, only disordered Si nanostructures were formed on the Si surface (Fig. 2c). According to our previously proposed mechanism for the formation of Si nanostructures in HF/Fe(NO<sub>3</sub>)<sub>3</sub> solution,<sup>[14]</sup> the SiO<sub>2</sub> or Si underneath the Ag particles is etched away by HF immediately, and the Ag particles enter the pits as they are forming. When the Ag particles are small, their lift-off or Brownian movement may occur during silicon dissolution, resulting in disordered Si structures. In contrast, stable Ag particles would facilitate the formation of 1D Si nanostructures. In addition, a higher HF concentration in the HF/Fe(NO<sub>3</sub>)<sub>3</sub> solution can greatly affect the etching reaction, and produce a disordered, porous morphology (Fig. 2d). Fe(NO<sub>3</sub>)<sub>3</sub> acts as a mild oxidant, and slightly affects the etching morphology, and could be replaced with other mild oxidants, such as Ni(NO<sub>3</sub>)<sub>2</sub> or Mg(NO<sub>3</sub>)<sub>2</sub>. We also performed some experiments to investigate the effect of gravity on the morphology of the etched Si wafers. We found that vertically aligned SiNW arrays could also be created on the surface of up-ended and upright Si wafers. Therefore, we suggest that any effects of gravity can be almost neglected in the present experiments.

Currently, there is substantial interest in the fabrication of antireflective surface structures in order to increase the energy-conversion efficiency of Si solar cells. Chemical and dry etching methods have been widely investigated to obtain desirably textured Si microstructures. Here, the as-synthesized black SiNWs samples on single-crystalline and multicrystalline Si wa-

fers show excellent antireflection ability, and could suppress light reflection over a wide spectral bandwidth. The reflectance of the SiNW arrays is less than 1.46% over the range 300–600 nm. This remarkable property suggests the as-synthesized large-area SiNW arrays as candidates for antireflective surface structures.

## 2.2. Formation of Si Nanostructures Using Other Noble Metals

The role of Ag may apply to other noble metals with a higher electronegativity than silicon. On a Si surface, these noble metals would attract electrons from the silicon and facilitate Si oxidation. Therefore, other noble-metal nanoparticles, including Au, Pt, and Cu, were investigated to clarify the role of Ag nanoparticles in the formation of SiNW arrays.

The SEM images in Figure 3 show the morphology of the electroless Au deposits on Si substrates, formed in an aqueous HF/KAuCl<sub>4</sub> solution, with different deposition times, and their influence upon the etched Si morphologies formed in the HF/Fe(NO<sub>3</sub>)<sub>3</sub> solution. Well-oriented SiNW arrays could be produced on Si substrates. A Au film composed of a high density of particles generally facilitates the formation of dense SiNW arrays. Many Au nanoparticles were found at the interface between the produced SiNWs and the Si substrate in the cross-sectional SEM image. This is similar to the cases found in SiNW samples prepared by Ag-seed-induced etching. All these results further imply that the possible sinking of metal nanoparticles into bulk silicon may play an important role in the formation of the SiNW arrays.

In contrast with the formation of SiNW arrays in the case of Ag- and Au-seed-induced chemical etching, no SiNWs were formed in the Pt-, Cu-, and Pd-seed-induced chemical etching in HF/Fe(NO<sub>3</sub>)<sub>3</sub> solution under our present experimental con-

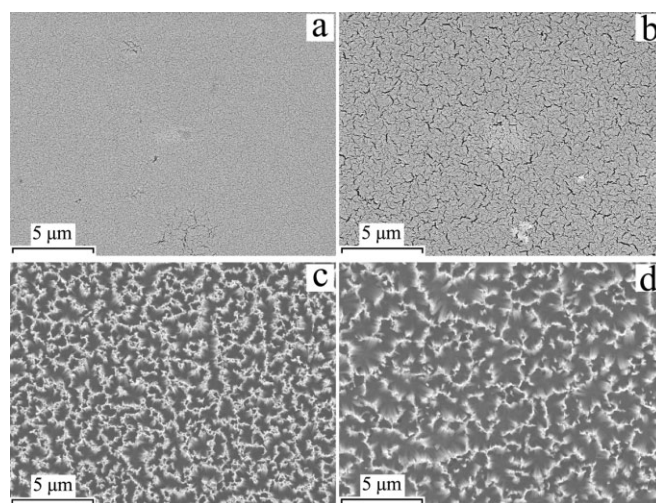


**Figure 3.** SEM images of the morphology of electroless Au deposits on a Si substrate from an aqueous HF/KAuCl<sub>4</sub> solution, after deposition times of a) 10 s and b) 30 s. c) SiNW arrays prepared on a Si substrate (after 10 s in HF/KAuCl<sub>4</sub>). d) SiNW arrays prepared on a Si substrate (after 30 s in HF/KAuCl<sub>4</sub>).

ditions. Unlike the electroless Ag and Au deposition, dispersed Pt nanoparticles, with large spaces between the particles, were always formed on the Si surface from aqueous HF/K<sub>2</sub>PtCl<sub>6</sub> solution (Fig. 4a). When a Pt-covered Si substrate was immersed into a HF/Fe(NO<sub>3</sub>)<sub>3</sub> solution, only separated, deep pores were created (Fig. 4b); in other words, porous silicon microstructures instead of 1D Si nanostructure arrays were obtained in

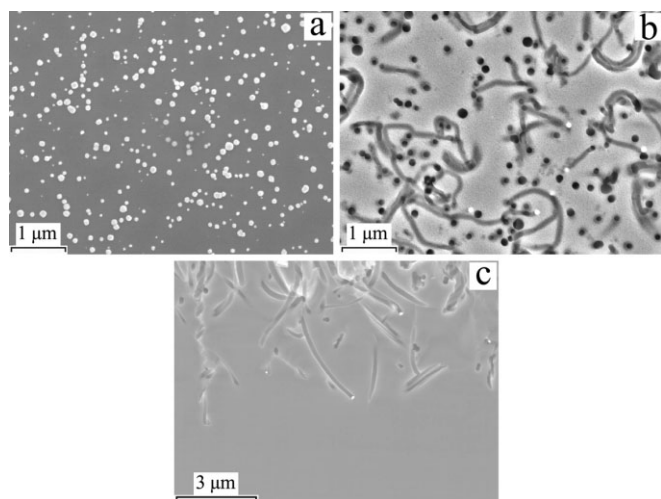


**Figure 4.** a) Dispersed Pt particles formed on a Si surface from aqueous HF/K<sub>2</sub>PtCl<sub>6</sub> solution. b) Porous silicon prepared with a Pt-treated Si substrate in HF/Fe(NO<sub>3</sub>)<sub>3</sub> solution. c) SEM cross-sectional image of the as-synthesized sample, with Pt particles situated at the interface.

the case of Pt-assisted chemical etching of Si wafers. SEM cross-sectional observations of as-synthesized samples with Pt nanoparticles showed that Pt nanoparticles sank into the bulk silicon, and were pinned at the bottom of the pores within the bulk silicon (Fig. 4c). The sinking tracks of Pt nanoparticles constitute the deep pores, as observed in Figure 4b. In the case of Pt-assisted etching of silicon, although deep nanoholes could be generated, they were not as straight as those obtained with the Ag and Au nanoparticles. Therefore, vertically aligned SiNW arrays could not be produced in case of Pt-assisted etching of silicon. However, the intrinsic difference in the catalytic activity between Ag and Pt is not yet clear.

Only shallow pits were formed on the Si surface when Cu seeds were used, and no Cu particles were observed after treatment in HF/Fe(NO<sub>3</sub>)<sub>3</sub> solution (Fig. 5b). The Cu may have

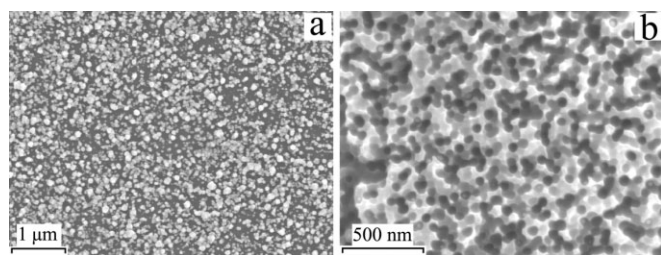


**Figure 5.** a) SEM image of Cu particles on silicon from HF/Cu(NO<sub>3</sub>)<sub>2</sub> solution. b) Shallow pits formed on a Cu-treated Si substrate.

disappeared from the aqueous HF/Fe(NO<sub>3</sub>)<sub>3</sub> solution because the standard redox potential of Cu/Cu<sup>2+</sup> is lower than that of Fe<sup>3+</sup>/Fe<sup>2+</sup>: Cu nanoparticles would dissolve into the solution as soluble Cu<sup>2+</sup> ions, according to Equation 1.

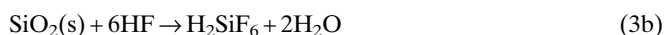
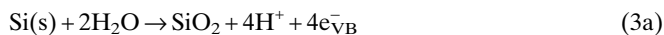


### 2.3. Formation Mechanism of SiNW Arrays

The generally accepted growth mechanism of SiNWs is the vapor–liquid–solid (VLS) growth mechanism, which is based on the growth from a liquid metal–seed particle.<sup>[4,17]</sup> Obviously, the formation mechanism of the as-synthesized SiNW arrays is quite different from previously proposed mechanisms. To clarify the formation mechanism of the SiNWs, we must have a full knowledge of EMD and the behavior of metals in hydrofluoric acid solution.

The electroless deposition of metals on silicon from fluoride solutions has raised considerable interest, owing to its wide application in microelectronics.<sup>[13]</sup> The working principle is the galvanic displacement reaction; that is, the reduction of metal ions (cathodic process) and the oxidation of Si atoms (anodic process) occur simultaneously at the Si surface, while the charge is exchanged through the Si substrate. Generally, the galvanic displacement reaction on Si with Ag, Au, and Pt salts with highly positive equilibrium reduction potentials is expected to occur by the injection of holes into the valence band (VB).<sup>[18]</sup> The silicon–silicon bonds supply the electrons used to reduce the metal salts on the Si surface, which, in the presence of HF, leads to the subsequent dissolution of the Si substrate.

Taking, for example, the electroless deposition of Ag in HF/AgNO<sub>3</sub> solution, we will try to explain the galvanic displacement reaction, according to the experimental results presented here and a previous report.<sup>[14]</sup> In the case of electroless deposition of Ag on silicon from HF/AgNO<sub>3</sub> solution, the energy levels of the Ag<sup>+</sup>/Ag system lie well below the Si VB edge, and the reduction of Ag<sup>+</sup> ions is not limited by the minority carrier concentration, owing to the presence of bonding electrons (Fig. 6). Simultaneous electrochemical processes including cathodic and anodic reactions occur on the Si surface exposed to the fluoride solution containing Ag<sup>+</sup> ions. Surface Si atoms are oxidized (anodic reaction) and supply the electrons for the Ag<sup>+</sup> reduction (cathodic reaction). The corresponding reaction can be outlined by the two half-cell reactions: Equation 2 (cathode reaction) and Equations 3a,b (anode reaction, which occurs underneath Ag nanoparticles)



However, these chemical reactions do not give us any information about Ag nucleation, Ag-particle growth, or Si dissolution.

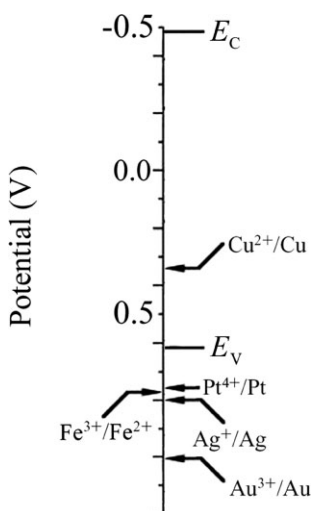


**Figure 6.** Qualitative diagram of the comparison between the electrochemical electron energy levels of the Si band edges ( $E_c$  and  $E_v$  are the conduction and valence bands, respectively) and five redox systems, including  $\text{AuCl}_4^-/\text{Au}$ ,  $\text{PtCl}_6^{2-}/\text{Pt}$ ,  $\text{Ag}^+/\text{Ag}$ ,  $\text{Cu}^{2+}/\text{Cu}$ , and  $\text{Fe}^{3+}/\text{Fe}^{2+}$ , in HF solution.

In order to explore the formation mechanism of SiNWs in HF/AgNO<sub>3</sub> solution, we must understand where the oxidation and dissolution of the Si substrate occur during the electroless Ag deposition. Do they occur from beneath the Ag deposits, or alongside them as we previously proposed?<sup>[15]</sup> Our present experimental results, especially the cross-sectional SEM observations, indicate that the oxidation and dissolution of the Si substrate do not occur alongside the Ag deposits, but beneath them. Morinaga et al.<sup>[19a]</sup> and Kim et al.<sup>[19b]</sup> have reported that electrochemical Cu deposition simultaneously accompanies the localized oxidation and dissolution of silicon, which take place underneath the deposited Cu and induces pits in the same position as a result of etching with dilute HF solution. Recently, Mitsugi and Nagai reported pit formation induced by Cu contamination in dilute HF solution.<sup>[20]</sup> They proposed that the local redox couple between Cu and the nearby Si surface is essential to the formation of localized pits, which were formed at the same position as the Cu islands.

According to these reports and our experimental results, we believe that the Si/AgNO<sub>3</sub>/HF system is composed of a corrosion-type redox couple: the cathodic reduction of Ag<sup>+</sup> ions and its counterpart, the anodic oxidation and dissolution of silicon, which occurs locally beneath the Ag deposits. In the initial stages of silver deposition, Ag<sup>+</sup> ions in the vicinity of the silicon surface capture electrons from the VB of Si, and are deposited in the form of metallic Ag nuclei on a nanoscopic scale (Fig. 7); generally, electron exchange between Ag<sup>+</sup> ions and Si is more likely to take place at kinks, steps, and other defects. As the Ag nuclei adhering to the Si surface are more electronegative than Si, these metallic Ag nuclei strongly attract electrons from Si and become negatively charged. These Ag nuclei serve to catalyze the subsequent reduction of Ag ions, and facilitate Si oxidation. Therefore, other Ag<sup>+</sup> ions coming close to the Si surface preferentially get electrons from the Ag nuclei, and are deposited around them. Thus, the Ag nuclei grow into

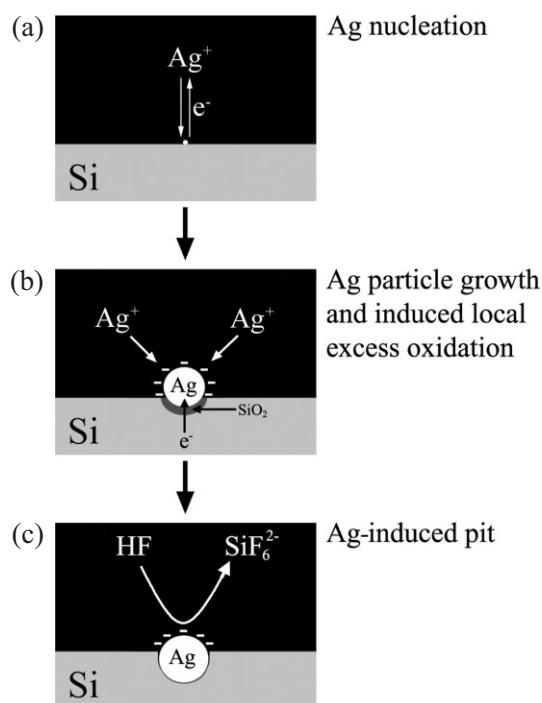


**Figure 7.** Mechanism of electroless Ag deposition on a Si substrate in HF/AgNO<sub>3</sub> solution.

larger particles as more Ag ions are deposited. Simultaneously, because the Si underneath the Ag particles releases as many electrons as are required by Ag ions to be reduced, excess local oxidation occurs, and SiO<sub>2</sub> is produced underneath these Ag nanoparticles. Shallow pits would immediately form underneath the Ag nanoparticles, due to the etching of SiO<sub>2</sub> by the HF solution; then the Ag particles enter the forming pits (Fig. 7). Therefore, the Ag particles trapped in these pits do not move horizontally. This illustration is consistent with our SEM observations, which confirmed that the oxidation and dissolution of the Si substrate occurred from beneath the Ag particles that are trapped in the formed pits. With longer immersion times in the HF/AgNO<sub>3</sub> solution, the Ag particles that do not enter the pits would grow into branched silver dendrites, as we found previously.<sup>[15]</sup>

The energy levels of the Fe<sup>3+</sup>/Fe<sup>2+</sup> system in HF/Fe(NO<sub>3</sub>)<sub>3</sub> solution lie well below the VB of silicon, so they more likely interact with the VB bonding electrons of silicon, and active kinetics are expected for the electron-capture process. The oxidizing agent Fe<sup>3+</sup> could gain electrons either by withdrawing them from silicon or by hole injection. The injection of holes from the Fe<sup>3+</sup>/Fe<sup>2+</sup> system into the silicon corresponds to the negative current (cathode process). The cathodic current density on p-type silicon immersed in HF/Fe(NO<sub>3</sub>)<sub>3</sub> solution can be described by Equation 4<sup>[20]</sup>

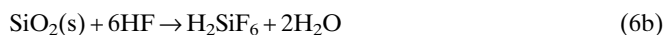
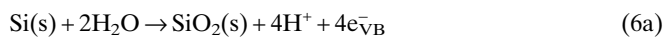
$$j_c = -ze k_c n_{Sc_{ox}} \exp(-E_a/k_B T) \quad (4)$$

where  $j_c$  is the cathodic current density,  $z$  is the number of electrons transferred during the reaction,  $e$  is the charge of an



electron,  $k_c$  is the rate constant,  $n_s$  is the electron density at the Si/HF/Fe(NO<sub>3</sub>)<sub>3</sub> solution interface,  $c_{ox}$  is the concentration of oxidant at the interface,  $E_a$  is the activation energy for the cathodic reaction,  $k_B$  is the Boltzmann constant, and  $T$  is the absolute temperature. A similar equation holds for the n-type silicon.

The oxidation and dissolution of silicon in HF/Fe(NO<sub>3</sub>)<sub>3</sub> solution proceed very slowly at a temperature as low as 50 °C in the absence of metal nanoparticles. However, covering the Si surface with Ag or other noble-metal nanoparticles greatly enhances the etching reaction. Metal contamination on the silicon surface has a strong catalytic activity for the cathodic reaction; furthermore, it is more electronegative than silicon. The catalytic activity of these metal species can be interpreted as a decrease in  $E_a$  for the cathodic reaction. Therefore, the accelerated dissolution of silicon can be explained by the enhanced cathodic reaction, due to the presence of Ag nanoparticles on the Si surface. According to our previous report,<sup>[14]</sup> the Ag particles can act as stable, local microcathodes (for the reduction of Fe<sup>3+</sup> ions), owing to the more positive redox potential of the Ag<sup>+</sup>/Ag system compared to the Fe<sup>3+</sup>/Fe<sup>2+</sup> couple, and reduce  $E_a$  for the cathodic reaction. The above reaction can be outlined by the two half-cell reactions shown in Equation 5 (cathodic reaction at the Ag nanoparticles) and Equations 6a,b (anodic reaction underneath the Ag nanoparticles)



Therefore, in the Ag/Si/HF/Fe(NO<sub>3</sub>)<sub>3</sub> system, the Fe<sup>3+</sup> ions have a strong tendency to obtain electrons preferentially from Ag particles and be reduced to Fe<sup>2+</sup> ions, while the silicon underneath the Ag nanoparticles is locally oxidized into SiO<sub>2</sub>. The reaction proceeds as long as the Si atoms are able to dissolve into the solution, or until thick SiO<sub>2</sub> forms, thereby halting electron transfer. In the present HF/Fe(NO<sub>3</sub>)<sub>3</sub> solution, the dissolution rate of SiO<sub>2</sub> by HF is higher than the Si oxidation rate by Fe(NO<sub>3</sub>)<sub>3</sub>. Therefore, the Si surface is always exposed to the solution. Figure 8 shows a schematic illustration for the possible SiNW array formation process on an Ag-treated Si substrate in HF/Fe(NO<sub>3</sub>)<sub>3</sub> solution.

As Ag nanoparticles are pinned by the pits and cannot move horizontally on the silicon surface, local etching in the close vicinity of Ag nanoparticles occurs, and deeper pits form owing to the continuous etching away of the SiO<sub>2</sub> underneath the Ag particles and the sinking of the Ag nanoparticles with prolonged immersion in the HF/Fe(NO<sub>3</sub>)<sub>3</sub> solution. The deep pits are simply the sinking tracks of Ag nanoparticles. For highly dispersed metal nanoparticles, separated, deep pores should form. However, deposited Ag particles have a strong tendency to form dense, interconnected networks under the present Ag deposition conditions. The collective sinking of the Ag particle networks would scratch the Si surface, and give rise to the formation of porous silicon. The subsequent dissolution of the thin pore walls would result in the final formation of freestand-

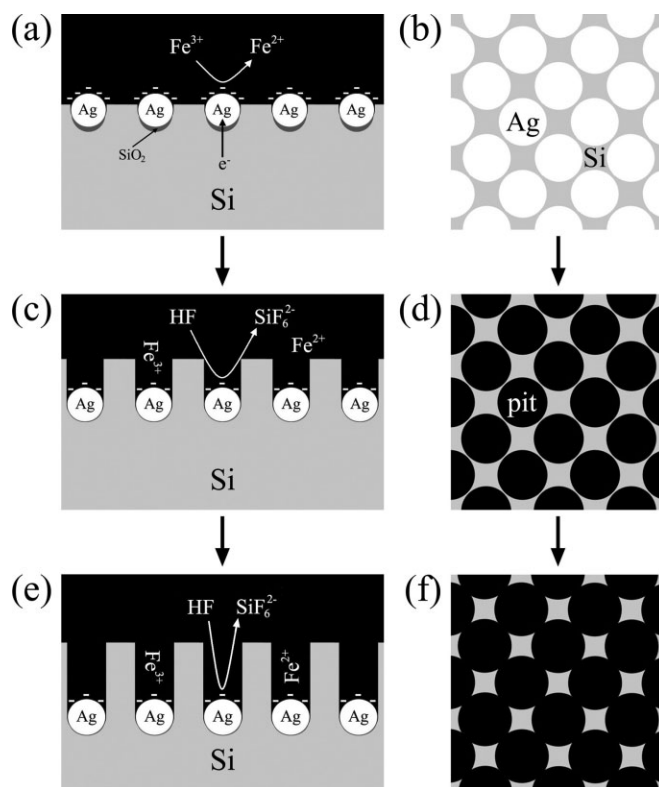


**Figure 8.** Schematic cross-sectional and planar views of SiNW array formation on a Ag-treated Si substrate in HF/Fe(NO<sub>3</sub>)<sub>3</sub> solution. a,b) Charge exchange between Si atoms and Fe<sup>3+</sup> ions preferentially occurs on Ag particles, and induces local oxidation of the Si substrate. c,d) Local dissolution of the oxidized Si substrate and simultaneous pitting at the same position causes the formation of interconnected, porous silicon. e,f) Formation of SiNW arrays due to the further sinking of the Ag particles, and longitudinal and lateral dissolution of bulk Si.

ing, 1D Si nanostructures, including nanowires and nanoribbons. Deeper pits, or long, thinner SiNWs would be produced if the Ag- or Au-particle-covered Si wafers were continuously immersed in the HF/Fe(NO<sub>3</sub>)<sub>3</sub> solution. The etching of silicon would continue until the supply of oxidizing Fe<sup>3+</sup> ions was exhausted. Therefore, the mechanism proposed here is very similar to that proposed by Canham.<sup>[21]</sup> Separate straight nanoholes could be created in silicon wafers if the silicon surface were patterned with separated, stable metal particles. Our present experiments have proven that well-ordered nanohole patterns can be prepared on patterned Si substrates that are covered with a pattern of Ag particles.

Recently, we prepared similar SiNW arrays in aqueous HF/AgNO<sub>3</sub> solution, and proposed one self-assembling nanoelectrochemistry mechanism for the formation of SiNW arrays.<sup>[15]</sup> However, owing to the strong reaction between silicon and solutions of HF/AgNO<sub>3</sub>, as well as a mass of silver dendrites produced by the galvanic displacement reaction, the intrinsic reaction mechanism is not easily accessible, and the proposed mechanism is short of convincing experimental evidence. Fortunately, our present experiments presented an opportunity to survey the mechanism proposed for SiNWs in aqueous HF/AgNO<sub>3</sub> solution again. So we systemically investi-

gated the morphological evolution of a p-type Si(111) wafer in HF/AgNO<sub>3</sub> solution. In the initial stages, only Ag nanoparticles formed on the Si surface. With the elapse of treatment time, some Ag particles gradually dug pits into the bulk silicon, and some other, large Ag particles began to form branched dendrites; simultaneously, large quantities of nanoscale Si needles protruded outward from the interspaces between the Ag particles on the Si surface. These phenomena imply that the appearance of Si needles may be ascribed to the sinking of Ag particles into bulk silicon, because the “growth” of Si needles is impossible in this case. Therefore, the formation mechanism of SiNWs in HF/AgNO<sub>3</sub> solution should be identical to the present mechanism for SiNWs formed in HF/Fe(NO<sub>3</sub>)<sub>3</sub> solution.

Another important question is why lateral etching does not occur. In our present experiments, the pore diameter was determined by the size of the metal particle. With the dissolution of silicon and the reduction of Fe<sup>3+</sup> ions, a charge-depletion layer (Fig. 9) with high resistance would emerge around the metal particles. Therefore, the metal site where electrons are consumed, and the silicon site where electrons are released, should not be far apart in order to realize the direct transport of electrons. We suggest that the charge exchange and transport between the anodic and cathodic sites would be more favorable at the metal/Si interface than at the pit wall, because the metal/Si interface has the shortest charge-transport distance, and because of the unique catalytic property of the metal particle, which greatly decreases  $E_a$  for the cathodic reaction (Fig. 9). Accordingly, oxide formation and the dissolution of silicon would more favorably occur at the pore tips (the metal/Si interface) than at the pit walls. That is, longitudinal etching would be more favored than lateral etching; thus, deep pores would be finally formed, owing to the prolonged longitudinal etching of silicon. In addition, if the metal particles were close to each other, the produced pores would have a great possibility of coalescing into one pore with a large diameter, which has been proven by our SEM observations. However, as mentioned above, a puzzling problem is that the pores generated with stable Pt particles were not as straight as those obtained with Ag and Au particles. Therefore, the nature and propagation of the Si/metal interface during Si oxidation and dissolution

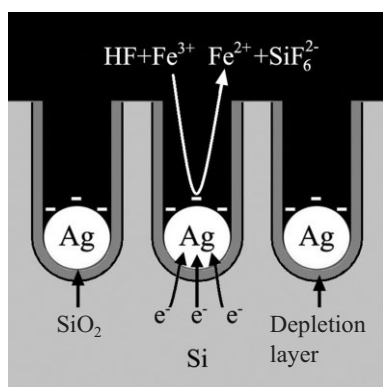


**Figure 9.** Mechanism of hindering the lateral dissolution of silicon along the pore during metal catalytic etching in HF solution.

should be addressed to clarify the novel etching mechanism. However, experimentally studying the interface propagation on an atomic scale during etching is very difficult, and perhaps not yet possible. Theoretical microscopic dynamic simulations may supply some useful information about the advancing Si/metal interface structure.

### 3. Conclusion

We have demonstrated a simple technique for rapidly producing large-area, highly oriented SiNW arrays on Si wafers by scratching the Si surface with metal particles at near room temperature. The etching technique shows little dependence on the orientation or doping type of the Si wafer. Therefore, SiNWs with desirable axial crystallographic orientation and doping characteristics could be readily obtained. The remarkable antireflection property of the produced SiNWs films also indicates their potential applicability as an antireflective layer for photovoltaic devices and optical detectors. A reasonable mechanism has been proposed on the basis of the electrochemistry of silicon and convincing experimental evidence.

### 4. Experimental

The synthesis of SiNW arrays was conducted in a sealed Teflon vessel. The production process comprised three steps: i) the Si wafers were cleaned by being soaked in acetone for five minutes and then ethanol for five minutes; they were then rinsed with de-ionized water two or three times, soaked in H<sub>2</sub>SO<sub>4</sub>/H<sub>2</sub>O<sub>2</sub> [H<sub>2</sub>SO<sub>4</sub> (97 %)/H<sub>2</sub>O<sub>2</sub> (30 %) = 3:1] for ten minutes, thoroughly rinsed with deionized water, and finally dipped in HF solution for one minute; ii) the metal nanoparticles were electroplated onto the cleaned Si surface; and iii) the metal-treated Si wafers were immersed in HF-based aqueous chemical etching solutions, then sealed and treated at 50 °C. The obtained samples were rinsed copiously with de-ionized water, and dried at room temperature. The length of SiNWs could be effectively controlled by adjusting the etching time.

The deposition of various metals, including Ag, Au, Pt, and Cu, on silicon was investigated. The concentrations of HF and AgNO<sub>3</sub> for depositing a Ag-nanoparticle film were 4.6 and 0.01 M, respectively. The concentrations of HF and Fe(NO<sub>3</sub>)<sub>3</sub> for etching metal-nanoparticle-covered silicon wafers were 4.6 and 0.135 M, respectively. The concentrations of HF and KAuCl<sub>4</sub> for depositing Au-nanoparticle film were 6.0 and 0.005 M, respectively. The concentrations of HF and K<sub>2</sub>PtCl<sub>6</sub> for depositing Pt-nanoparticle film were 6.0 and 0.007 M, respectively.

The as-synthesized samples were studied using SEM (JEOL 6301F) and TEM (JEOL 2010F) with the microscope equipped with an energy-dispersive X-ray spectrometer and a Gatan GIF 678 system. To prepare specimens for TEM analysis, the samples were scraped using a knife, and the scrapings were collected and suspended in ethanol. A drop of the ‘solution’ was placed on a carbon-coated copper grid and examined using a JEOL 2010F microscope.

Received: June 25, 2005  
Final version: August 24, 2005  
Published online: December 8, 2005

- [1] S. Iijima, *Nature* **1991**, 354, 56.  
[2] a) M. Law, J. Goldberger, P. D. Yang, *Annu. Rev. Mater. Res.* **2004**, 34, 83. b) M. Law, D. J. Sirbully, J. C. Johnson, J. Goldberger, R. J. Saykally, P. D. Yang, *Science* **2004**, 305, 1269. c) X. F. Duan, Y. Huang,

- R. Agarwal, C. M. Lieber, *Nature* **2003**, *421*, 241. d) X. F. Duan, Y. Huang, Y. Cui, J. F. Wang, C. M. Lieber, *Nature* **2001**, *409*, 66. e) Z. L. Wang, *Annu. Rev. Phys. Chem.* **2004**, *55*, 159. f) K. Q. Peng, Z. P. Huang, J. Zhu, *Adv. Mater.* **2004**, *16*, 73. g) Y. Huang, X. F. Duan, C. M. Lieber, *Small* **2005**, *1*, 142. h) S. Mathur, S. Barth, H. Shen, J. C. Pyun, U. Werner, *Small* **2005**, *1*, 713. i) K. Q. Peng, Y. Xu, Y. Wu, Y. J. Yan, S. T. Lee, J. Zhu, *Small* **2005**, *1*, 1062. j) P. D. Yang, H. Q. Yan, S. Mao, R. Russo, J. Johnson, R. Saykally, N. Morris, J. Pham, R. R. He, H. J. Choi, *Adv. Funct. Mater.* **2002**, *12*, 323. k) Z. L. Wang, X. Y. Kong, Y. Ding, P. X. Gao, W. L. Hughes, R. S. Yang, Y. Zhang, *Adv. Funct. Mater.* **2004**, *14*, 329.
- [3] a) E. Leobandung, L. J. Guo, Y. Wang, S. Y. Chou, *Appl. Phys. Lett.* **1995**, *67*, 938. b) H. Ishikuro, T. Hiramoto, *Appl. Phys. Lett.* **1997**, *71*, 3691. c) B. Delley, E. F. Teigmeier, *Phys. Rev. B* **1993**, *47*, 1397. d) L. T. Canham, W. Y. Leong, M. I. J. Beale, T. I. Cox, L. Taylor, *Appl. Phys. Lett.* **1992**, *61*, 2563. e) T. K. Sham, D. T. Jiang, I. Coulthard, J. W. Lorimer, X. H. Feng, K. H. Tan, S. P. Frigo, R. A. Rosenberg, D. C. Houghton, B. Bryskiewicz, *Nature* **1993**, *363*, 331. f) C. Delerue, G. Allan, M. Lannoo, *Phys. Rev. B* **1993**, *48*, 11024. g) D. P. Yu, Z. G. Bai, J. J. Wang, Y. H. Zou, W. Qian, J. S. Fu, H. Z. Zhang, Y. Ding, G. C. Xiong, L. P. You, J. Xu, S. Q. Feng, *Phys. Rev. B* **1999**, *59*, R2498. h) R. J. Needs, S. Bhattacharjee, K. J. Nash, A. Qteish, A. J. Read, L. T. Canham, *Phys. Rev. B* **1994**, *50*, 14223. i) F. Buda, J. Kohanoff, M. Parrinello, *Phys. Rev. Lett.* **1992**, *69*, 1272. j) D. C. Lee, T. Hanrath, B. A. Korgel, *Angew. Chem. Int. Ed.* **2005**, *44*, 3573. k) J. H. Warner, A. Hoshino, K. Yamamoto, R. D. Tilley, *Angew. Chem. Int. Ed.* **2005**, *44*, 4550. l) J. Heitmann, F. Muller, M. Zacharias, U. Gosele, *Adv. Mater.* **2005**, *17*, 795.
- [4] J. Westwater, D. P. Gosain, S. Tomiya, S. Usui, H. Ruda, *J. Vac. Sci. Technol. B* **1997**, *15*, 554.
- [5] A. M. Morales, C. M. Lieber, *Science* **1998**, *279*, 208.
- [6] N. Wang, Y. F. Zhang, Y. H. Tang, C. S. Lee, S. T. Lee, *Appl. Phys. Lett.* **1998**, *73*, 3902.
- [7] D. P. Yu, Z. G. Bai, Y. Ding, Q. L. Hang, H. Z. Zhang, J. J. Wang, Y. H. Zou, W. Qian, G. C. Xiong, H. T. Zhou, S. Q. Feng, *Appl. Phys. Lett.* **1998**, *72*, 3458.
- [8] Y. F. Zhang, Y. H. Tang, C. Lam, N. Wang, C. S. Lee, I. Bello, S. T. Lee, *J. Cryst. Growth* **2000**, *212*, 115.
- [9] J. D. Holmes, K. P. Johnston, R. C. Doty, B. A. Korgel, *Science* **2000**, *287*, 1471.
- [10] K. Q. Peng, J. Zhu, *J. Electroanal. Chem.* **2003**, *558*, 35.
- [11] Y. Cui, L. J. Lauhon, M. S. Gudiksen, J. F. Wang, C. M. Lieber, *Appl. Phys. Lett.* **2001**, *78*, 2214.
- [12] a) *Electrochemistry of Silicon: Instrumentation, Science, Materials and Applications* (Ed: V. Lehmann), Wiley-VCH, Weinheim, Germany **2002**. b) *Electrochemistry of Silicon and Its Oxide* (Ed: X. G. Zhang), Kluwer, Dordrecht, The Netherlands **2001**.
- [13] a) P. Gorostiza, R. Diaz, J. Servat, F. Sanz, J. R. Morante, *J. Electrochem. Soc.* **1997**, *144*, 909. b) P. Gorostiza, M. A. Kulandainathan, R. Diaz, F. Sanz, P. Allongue, J. R. Morante, *J. Electrochem. Soc.* **2000**, *147*, 1026. c) S. Ye, T. Ichihara, K. Uosaki, *J. Electrochem. Soc.* **2001**, *148*, C421. d) G. J. Norga, M. Platero, K. A. Black, A. J. Reddy, J. Michel, L. C. Kimerling, *J. Electrochem. Soc.* **1997**, *144*, 2801. e) V. Bertagna, C. Plougonven, F. Rouelle, M. Chemla, *J. Electrochem. Soc.* **1996**, *143*, 3532. f) L. A. Porter, H. C. Choi, A. E. Ribbe, J. M. Buriak, *Nano Lett.* **2002**, *2*, 1067. g) C. Carraro, L. Magagnin, R. Maboudian, *Electrochem. Acta* **2002**, *47*, 2583. h) L. Magagnin, R. Maboudian, C. Carraro, *J. Phys. Chem. B* **2002**, *106*, 401.
- [14] K. Q. Peng, Y. Wu, H. Fang, X. Y. Zhong, Y. Xu, J. Zhu, *Angew. Chem. Int. Ed.* **2005**, *44*, 2737.
- [15] a) K. Q. Peng, Y. J. Yan, S. P. Gao, J. Zhu, *Adv. Mater.* **2002**, *14*, 1164. b) K. Q. Peng, Y. J. Yan, S. P. Gao, J. Zhu, *Adv. Funct. Mater.* **2003**, *13*, 127. c) K. Q. Peng, J. Zhu, *Electrochem. Acta* **2004**, *49*, 2563.
- [16] X. J. Li, D. L. Zhu, Q. W. Chen, Y. H. Zhang, *Appl. Phys. Lett.* **1999**, *74*, 389.
- [17] A. I. Hochbaum, R. Fan, R. R. He, P. D. Yang, *Nano Lett.* **2005**, *5*, 457.
- [18] a) I. Teerlinck, P. W. Mertens, H. F. Schmidt, M. Meuris, M. M. Heyns, *J. Electrochem. Soc.* **1996**, *143*, 3323. b) P. Gorostiza, R. Diaz, M. A. Kulandainathan, F. Sanz, J. R. Morante, *J. Electroanal. Chem.* **1999**, *469*, 48.
- [19] a) H. Morinaga, M. Suyama, T. Ohmi, *J. Electrochem. Soc.* **1994**, *141*, 2834. b) J. S. Kim, H. Morita, J. D. Joo, T. Ohmi, *J. Electrochem. Soc.* **1997**, *144*, 3275.
- [20] N. Mitsugi, K. Nagai, *J. Electrochem. Soc.* **2004**, *151*, G302.
- [21] L. T. Canham, *Appl. Phys. Lett.* **1990**, *57*, 1046.